The EMBO Journal (2011) 30, 1003–1011 | © 2011 European Molecular Biology Organization | Some Rights Reserved 0261-4189/11
www.embojournal.org

THE EMBO JOURNAL

EMBO open

TIM23-mediated insertion of transmembrane α-helices into the mitochondrial inner membrane

Salomé Calado Botelho[1], Marie Österberg[1], Andreas S Reichert[2,3], Koji Yamano[4], Patrik Björkholm[1], Toshiya Endo[4], Gunnar von Heijne[1,5,*] and Hyun Kim[1,6,*]

[1]Department of Biochemistry and Biophysics, Center for Biomembrane Research, Stockholm University, Stockholm, Sweden, [2]Mitochondriale Biologie, Zentrum für Molekulare Medizin, Goethe Universität Frankfurt am Main, Frankfurt am Main, Germany, [3]Mitochondrial Biology, Frankfurt Institute for Molecular Life Sciences, Frankfurt am Main, Germany, [4]Department of Chemistry, Graduate School of Science, Nagoya University, Nagoya, Japan, [5]Science for Life Laboratory Stockholm University, Solna, Sweden and [6]School of Biological Sciences, Seoul National University, Seoul, South Korea

While overall hydrophobicity is generally recognized as the main characteristic of transmembrane (TM) α-helices, the only membrane system for which there are detailed quantitative data on how different amino acids contribute to the overall efficiency of membrane insertion is the endoplasmic reticulum (ER) of eukaryotic cells. Here, we provide comparable data for TIM23-mediated membrane protein insertion into the inner mitochondrial membrane of yeast cells. We find that hydrophobicity and the location of polar and aromatic residues are strong determinants of membrane insertion. These results parallel what has been found previously for the ER. However, we see striking differences between the effects elicited by charged residues flanking the TM segments when comparing the mitochondrial inner membrane and the ER, pointing to an unanticipated difference between the two insertion systems.

The EMBO Journal (2011) **30,** 1003–1011. doi:10.1038/emboj.2011.29; Published online 15 February 2011
Subject Categories: membranes & transport
Keywords: CoxVa; membrane protein; Mgm1p; mitochondria; TIM23

Introduction

The overwhelming majority of mitochondrial proteins are encoded on nuclear chromosomes, synthesized in the cytoplasm, and post-translationally imported into mitochondria through translocon complexes in the outer and inner membrane (Bolender *et al*, 2008). In the case of inner membrane proteins, two different translocons (TIM23, TIM22) can mediate membrane insertion of proteins arriving from the intermembrane space (IMS) side of the inner membrane, while the Oxa1p translocon inserts membrane proteins coming from the matrix side (Neupert and Herrmann, 2007; Becker *et al*, 2009).

The role of the TIM23 complex is analogous to that of the Sec61 translocon, which mediates translocation and insertion of proteins in the endoplasmic reticulum (ER) membrane (Rapoport, 2007; Skach, 2009). For both translocons, transmembrane (TM) segments are thought to be integrated into the lipid bilayer by lateral exit from the translocon pore (Becker *et al*, 2009; Skach, 2009). Despite the apparent functional similarities, the TIM23 and the Sec61 translocons are not evolutionarily related (Herrmann, 2003; Dolezal *et al*, 2006). Thus, it is unknown to what extent the two translocons use similar principles of recognizing TM segments in membrane proteins.

Here, we present an analysis of the sequence characteristics governing the insertion of membrane proteins by the TIM23 complex. To measure the efficiency of TM-segment insertion into the inner membrane, we have taken advantage of the peculiar maturation pathway of Mgm1p, a nuclearly encoded, dynamin-like GTPase important for mitochondrial fusion, morphology, and genome integrity in *Saccharomyces cerevisiae* (Sesaki *et al*, 2003; Wong *et al*, 2003; Sesaki and Jensen, 2004). Mgm1p is sorted into the inner membrane by the TIM23 complex through a unique process called alternative topogenesis (Herlan *et al*, 2004) (Figure 1A). Mgm1p has a classical N-terminal mitochondria-targeting presequence followed by two hydrophobic segments and a C-terminal globular domain. After cleavage of the presequence by the matrix processing peptidase, the first hydrophobic segment is inserted into the inner membrane in about half of the molecules. This gives rise to the long isoform of the protein (*l*-Mgm1p). In the remaining Mgm1p molecules, the first hydrophobic segment slips through the TIM23 channel into the matrix whereupon the second hydrophobic segment is cleaved by a rhomboid-like protease, Pcp1p, in the inner membrane (Herlan *et al*, 2003, 2004; Schäfer *et al*, 2010), releasing a truncated C-terminal part of Mgm1p (*s*-Mgm1p) to the IMS. Both isoforms are required for function (Meeusen *et al*, 2006).

Results

We reasoned that Mgm1p carrying an engineered hydrophobic segment (H-segment) in place of the first TM segment should give rise to the two isoforms in varying amounts,

*Corresponding authors. G von Heijne, Department of Biochemistry and Biophysics, Center for Biomembrane Research, Stockholm University, Stockholm 106 91, Sweden. Tel.: +46 816 2590; Fax: +46 815 3679; E-mail: gunnar@dbb.su.se or H Kim, Department of Biological Sciences, College of Natural Sciences, Seoul National University, Seoul 151747, South Korea. Tel.: +82 2880 4440; Fax: +82 2872 1993; E-mail: joy@snu.ac.kr

Received: 6 October 2010; accepted: 17 January 2011; published online: 15 February 2011

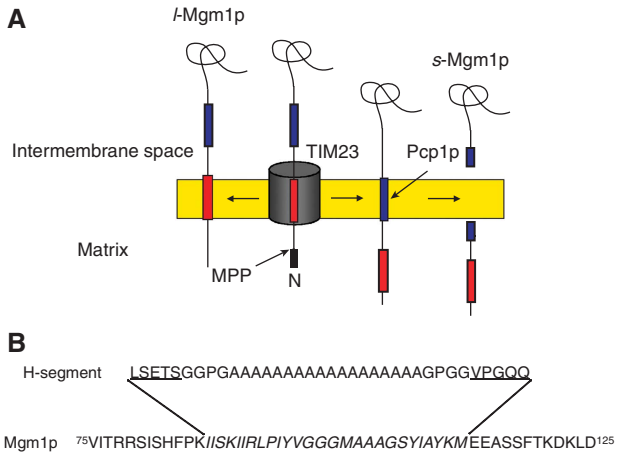

Figure 1 The Mgm1p model protein. (**A**) Alternative topogenesis of Mgm1p in the mitochondrial inner membrane (Herlan *et al*, 2004). Mgm1p is imported through the TIM23 translocon. The presequence (black) is cleaved by the matrix processing peptidase (MPP). The first hydrophobic segment (red) integrates into the membrane in about half of the molecules (left, *l*-Mgm1p). In the remaining molecules, the first hydrophobic segment translocates into the matrix, leaving the second hydrophobic segment (blue) spanning the membrane (right). The second segment is cleaved by the inner membrane protease Pcp1p, giving rise to *s*-Mgm1p. (**B**) The first hydrophobic segment of Mgm1p (residues 87–113, italics) was replaced by 37-residue long segments including an H-segment, its immediate flanking residues (GGPG…GPGG), and five additional flanking residues from H-segment constructs previously analysed in the ER (underlined).

depending on whether the H-segment is integrated into the inner membrane or not. We therefore replaced the first hydrophobic segment of Mgm1p by a set of 19-residue H-segments of varying hydrophobicity (Figure 1B), for which we have already measured membrane insertion in the mammalian and yeast ER (Hessa *et al*, 2007, 2009). For immunodetection, a triple-haemagglutinin (HA) tag was fused to the C-terminus of Mgm1p in all constructs. C-terminal epitope tagging of Mgm1p with either HA or c-*myc* does not compromise protein function (Meeusen *et al*, 2006; Zick *et al*, 2009) (and our unpublished data), showing that the C-terminal HA tag disrupts neither targeting nor topogenesis. Each Mgm1p construct was expressed in yeast from a low-copy *CEN* plasmid, and the relative amounts of the two isoforms were quantified from western blots and used to calculate an apparent free energy of membrane insertion, $\Delta G_{app} = -RT\ln(f_l/f_s)$ (where R is the gas constant and T is the absolute temperature, $T = 298$ K, and f_l and f_s denote the fractions of *l*-Mgm1p and *s*-Mgm1p molecules, respectively).

A hydrophobicity scale for mitochondrial inner membrane proteins

We first measured ΔG_{app} for a series of 19-residue Leu/Ala-based H-segments, with the composition GGPG-*n*L/(19-*n*)A-GPGG (all constructs are listed in Supplementary Table S1). The secondary-structure breaking GGPG…GPGG flanks were included to 'insulate' the H-segments from the surrounding protein sequence (Hessa *et al*, 2005). As anticipated, H-segments with a higher number of Leu residues produced a higher fraction of the membrane-anchored *l*-Mgm1p isoform relative to *s*-Mgm1p (Figure 2A). The measured ΔG_{app} is linear with the number of Leu residues (n), with $\Delta G_{app} = 0$ kcal/mol (50% membrane insertion) reached

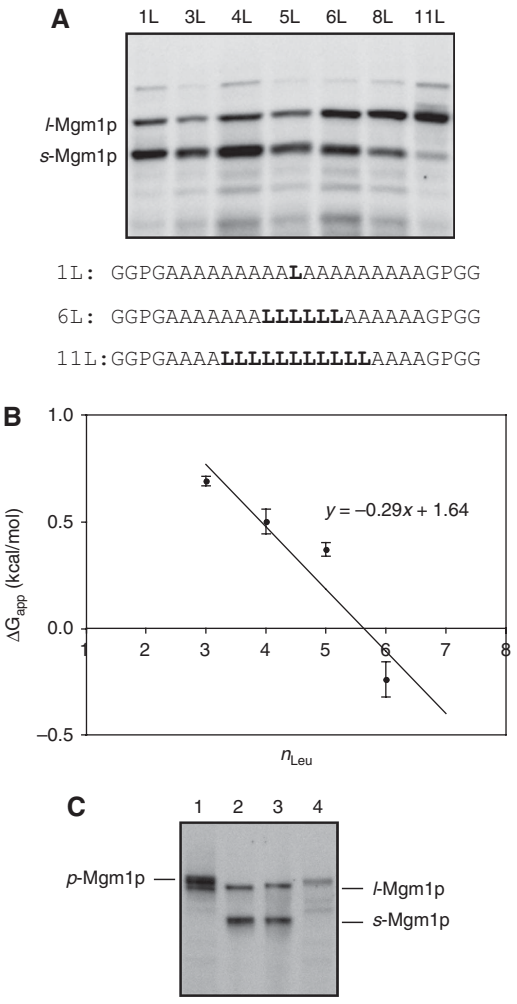

Figure 2 Membrane insertion efficiency of Leu/Ala-based H-segments. (**A**) Whole-cell lysates from yeast transformants expressing HA-tagged Mgm1p constructs with H-segments containing varying number of Leu residues were analysed by SDS–PAGE and western blotting. *l*-Mgm1p is the membrane-anchored long isoform and *s*-Mgm1p is the soluble short isoform. Three examples of H-segments are shown below the gel; all H-segment sequences are listed in Supplementary Table S1. (**B**) Membrane insertion efficiency expressed as ΔG_{app} plotted against the number of Leu residues in the H-segment. Averages from at least three independent experiments and standard errors are shown. (**C**) Western blot of *in vitro*-translated HA-tagged Mgm1p precursor (lane 1) and Mgm1p(6L/13A) precursor (lane 4), and of whole-cell lysate samples from yeast transformants expressing HA-tagged Mgm1p (lane 2) and Mgm1p(6L/13A) (lane 3). *p*-Mgm1p, *l*-Mgm1p, and *s*-Mgm1p denote, respectively, the precursor form, the long mature isoform, and the short mature isoform of HA-tagged Mgm1p.

for, $n \approx 5$–6 (Figure 2B). This 'threshold hydrophobicity' is increased by roughly one Ala→Leu replacement compared with the yeast ER (Hessa *et al*, 2009) and by two such replacements compared with the mammalian ER (Hessa *et al*, 2005). These differences may at least in part depend on charged residues outside the GGPG…GPGG flanks (see below).

As a control for proper mitochondrial import, we compared the size of the *l*-Mgm1p isoforms from whole-cell lysates prepared from yeast transformants carrying either HA-tagged Mgm1p or the HA-tagged Mgm1p(6L/13A) construct with the corresponding *in vitro*-translated full-length products (including the presequence) (Figure 2C).

A clear difference in molecular weight was observed between the *in vitro*-translated presequence-containing Mgm1p and the Mgm1p isoforms isolated from whole-cell lysates, indicating that the presequence has been cleaved from the Mgm1p constructs and therefore that they are correctly imported into the mitochondria.

To determine the contribution of each of the 20 naturally occurring amino acid to ΔG_{app}, we prepared a second set of H-segments (Supplementary Table S1). Each test amino acid was placed in the middle of the H-segment, so that it would be embedded in the hydrophobic core of the lipid bilayer when integrated into the membrane. As the maximal sensitivity of the assay is obtained when $\Delta G_{app} \approx 0$ kcal/mol (50% membrane insertion), the Ala/Leu composition of the H-segments was adjusted such that, for each test amino acid, the efficiency of insertion was not too far from 50%. Assuming a simple additive model for the contributions of Leu and Ala residues to ΔG_{app} for the 19-residue H-segments shown in Figure 2B, we have $\Delta G_{app} = n \cdot \Delta G_{app}^{Leu} + (19 - n) \cdot \Delta G_{app}^{Ala} = -0.29\ n + 1.64$ kcal/mol, which yields $\Delta G_{app}^{Leu} = -0.20$ kcal/mol and $\Delta G_{app}^{Ala} = 0.09$ kcal/mol. Possible contributions to ΔG_{app} from the Gly-Pro flanking sequences should be small (Hessa *et al*, 2005), and are ignored here. For the remaining 18 natural amino acids (X), ΔG_{app}^{X} was calculated from measured ΔG_{app} values as $\Delta G_{app}^{X} = \Delta G_{app} - (n \cdot \Delta G_{app}^{Leu} + (18 - n) \cdot \Delta G_{app}^{Ala})$, see Supplementary Table S1.

Figure 3A shows the mitochondrial ΔG_{app}^{X} scale. As expected, the hydrophobic amino acids are at the lower end of the scale, whereas the charged amino acids are found at the higher end. Comparison to the scale obtained for membrane insertion into the mammalian ER shows a good correlation ($R^2 = 0.81$) (Figure 3B), but the mitochondrial scale spans a somewhat broader range compared with the ER scale (−0.2 to +3.0 kcal/mol versus −0.5 to +1.8 kcal/mol) and the zero point is different, as noted above.

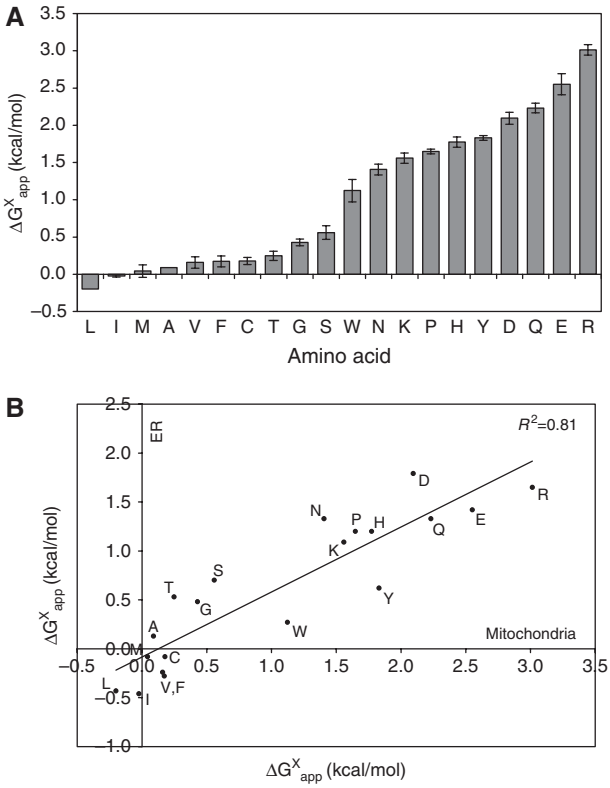

Figure 3 'Biological' ΔG_{app}^{X} scales. (**A**) The mitochondrial ΔG_{app}^{X} scale derived from Leu/Ala-based H-segments with the indicated amino acid placed in the middle of the H-segment (see Supplementary Table S1). Averages from at least three independent experiments and standard errors are shown. (**B**) Comparison between the ΔG_{app}^{X} scales obtained for the mitochondrial inner membrane and for the mammalian ER membrane (Hessa *et al*, 2007).

Position-dependent effects

Meier *et al* (2005) have reported that the presence of Pro residues in TM segments renders TIM23-mediated membrane insertion less efficient. To better understand the role of Pro in TM helix insertion, we analysed a set of H-segments carrying a single or a symmetrically disposed pair of Pro residues in different positions. As seen in Figure 4A and B, Pro residues strongly reduce membrane insertion when located in the middle section of the H-segment and to a lesser but significant extent when near the ends. This suggests that formation of an α-helical structure of the H-segment is an important determinant for TIM23-mediated recognition and insertion of the H-segment into the inner membrane.

We next assessed the positional dependence of the effects on membrane insertion elicited by pairs of aromatic residues (Phe, Trp, Tyr; Figure 4C) and by single-charged residues (Lys, Asp; Figure 4D). Membrane insertion increased when Trp and Tyr were placed near the ends of the H-segment, while the effect of Phe was largely independent of position. The positively charged Lys residue was found not to affect insertion compared with the parent 6L/13A H-segment when placed in the first or last four positions. These results are consistent with our previous findings for the mammalian ER (Hessa *et al*, 2007). In contrast, the negatively charged Asp residue was only tolerated when placed in the four C-terminal positions, whereas in the mammalian ER Asp is tolerated at both the N- and C-terminal ends of the H-segment.

Effects of charged and polar flanking residues

Finally, we investigated the role of charged and polar flanking sequences on H-segment insertion. On average, three positively charged Arg or Lys flanking residues (RRPR…, …RPRR, KKPK…, …KPKK) reduce ΔG_{app} by 1.0–1.3 kcal/mol from both the matrix and IMS sides compared with the GGPG… and …GPGG flanks (Figure 5). This corresponds to approximately four Ala→Leu replacements in the hydrophobic part of the H-segment.

In contrast, a negatively charged DDPD… flanking sequence on the matrix side increases ΔG_{app} by 1.1 kcal/mol, while a …DPDD sequence on the IMS side has little effect compared with the …GPGG flanking sequence, in agreement with the results for a single-Asp residue in Figure 4D. The same qualitative effects are seen with XXPX…,…XPXX flanking sequences where X = Glu, Gln, Asn, and His (see constructs #107–114, Supplementary Table S1); that is, it is not the charge *per se* but the high polarity of the side chain that matters in these cases. Interestingly, His does not behave as a positively charged residue in this context, which is consistent with the high pH of the mitochondrial matrix (around 8.0 in HeLa cells and rat cardiomyocytes (Llopis *et al*, 1998)), a value that is well above the pKa for the imidazole side chain.

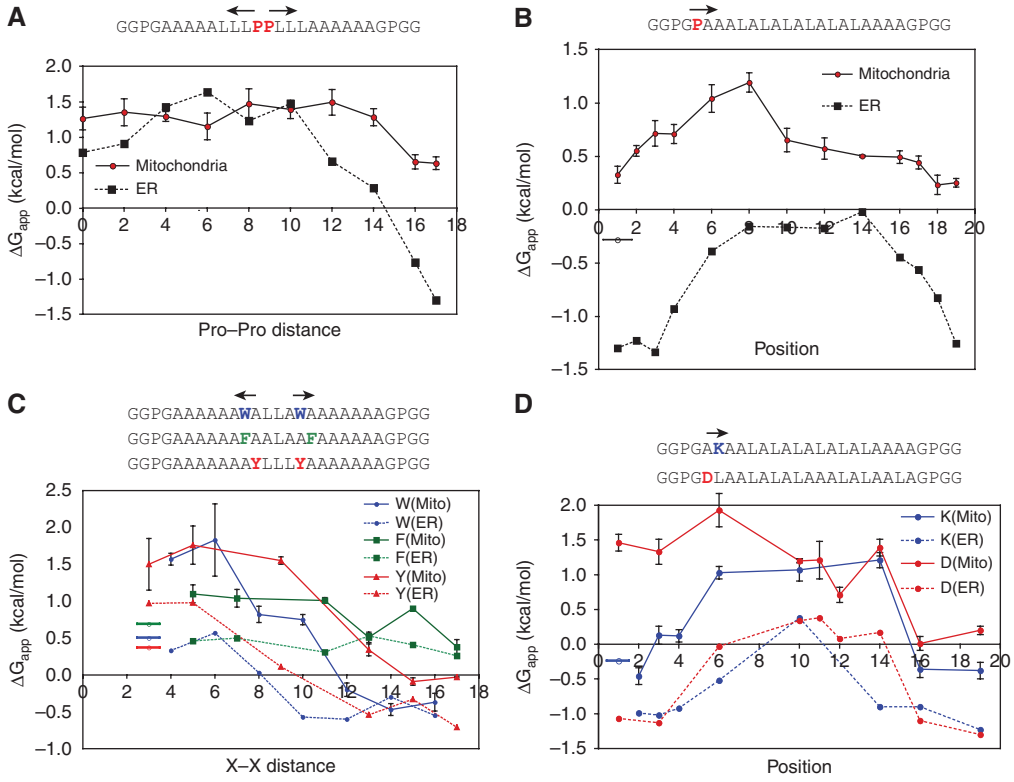

Figure 4 Position-dependent effects of different amino acids on membrane insertion. (**A**) Symmetric pair-scan for Pro residues in the mitochondrial inner membrane (circles) and the mammalian ER membrane (squares). (**B**) Single-Pro scan of H-segment insertion into the mitochondrial inner membrane (circles) and the mammalian ER membrane (squares). The ΔG_{app} value for the 6L/13A H-segment in the mitochondrial inner membrane is shown as a strikethrough circle. (**C**) Symmetric pair-scans for Trp (blue), Phe (green), and Tyr (red). Dashed lines show the corresponding data for the mammalian ER. The ΔG_{app} value (mitochondrial inner membrane) for the 3L/16A (green), 4L/15A (blue), and 5L/14A (red) H-segments are shown as strikethrough circles. (**D**) Lys (blue) and Asp (red) scans. Dashed lines show the corresponding data for the mammalian ER. The ΔG_{app} value (mitochondrial inner membrane) for the 6L/13A H-segment is shown as a strikethrough circle. In all panels, data points are averages from at least three independent experiments and standard errors are shown.

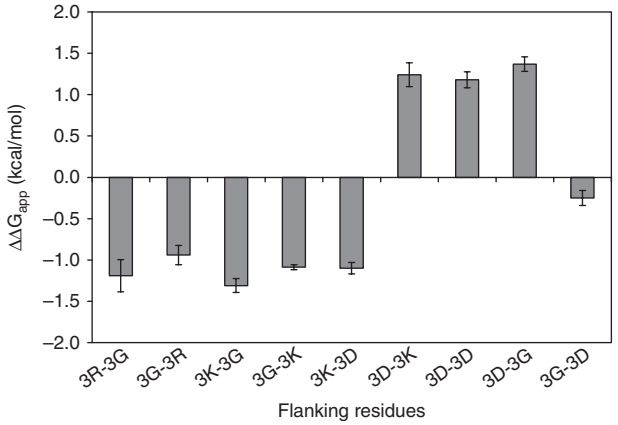

Figure 5 Effects of charged flanking residues on membrane insertion. Flanking sequences have the general design XXPX…XPXX (denoted 3X-3X) where X = G, R, K, or D. The results are expressed as $\Delta\Delta G_{app}$ values relative to the corresponding construct with GGPG…GPGG flanks. For the 3K-3G and 3G-3K flanks, the $\Delta\Delta G_{app}$ values have been averaged over multiple H-segments of different composition (see Supplementary Table S1). Averages from at least three independent experiments and standard errors are shown.

Positively charged residues thus promote membrane insertion from both sides of the membrane. This is in contrast to the mammalian ER, where positively charged residues only promote insertion if they are present on the cytoplasmic side of the H-segment (Hessa *et al*, 2007). Negatively charged and highly polar residues reduce membrane insertion only when placed at the matrix side of the H-segment in the mitochondrial system, and only when placed at the lumenal side of the H-segment in the mammalian ER (Hessa *et al*, 2007).

A second test protein: CoxVa

Given the importance of flanking residues located outside the hydrophobic segment itself and the relatively high threshold hydrophobicity for membrane insertion seen with the Mgm1p constructs, we also determined the threshold hydrophobicity using a second inner membrane protein, CoxVa. CoxVa has a single TM segment that is integrated into the inner membrane via the TIM23 translocon (Glaser *et al*, 1990; Miller and Cumsky, 1993). We replaced the CoxVa TM segment by GGPG-*n*L/(19-*n*)A-GPGG H-segments of varying hydrophobicity and determined the efficiency of membrane insertion by an established protease-accessibility assay (Glaser *et al*, 1990) (Figure 6A). As seen in Figure 6B, 50% membrane insertion is observed for $n \approx 2$–3, compared with $n \approx 5$–6 for Mgm1p, corresponding to a difference of $\sim$1 kcal/mol in the threshold hydrophobicity between the CoxVa and Mgm1p constructs. Although minor differences between *in vivo* and *in vitro* import assays may explain part of this difference (as has been seen for insertion into the ER (Hessa *et al*, 2005)),

it is likely that sequence context outside the GGPG…GPGG flanks also impact the threshold hydrophobicity.

Positively and negatively charged flanking residues have similar effects on membrane insertion in the context of CoxVa as seen for Mgm1p, that is, positively charged flanks tend to increase insertion while negatively charged flanking residues on the matrix side of the hydrophobic segment strongly reduce insertion (Figure 6C).

Impairment of import-motor function increases membrane insertion

Herlan *et al* (2004) have shown that mutational impairment of the mitochondrial import-motor components Tim44p and Pam18p/Tim14p reduces the formation of *s*-Mgm1p, implying that membrane integration of Mgm1p is increased in the absence of motor activity. We therefore tested the effect of the import motor on the balance between *s*-Mgm1p and *l*-Mgm1p in constructs with different H-segments. In case of wild-type Mgm1p, we observed a strong reduction of the amount of *s*-Mgm1p in the temperature-sensitive mutant *pam16-3* of the motor subunit Pam16p (Frazier *et al*, 2004) grown at 30°C, the highest temperature at which cells can still grow (Figure 7A). The relative levels of *s*-Mgm1p were reduced in *pam16-3* cells also for Mgm1p carrying H-segments of varying hydrophobicity, but to a smaller degree than for wild-type Mgm1p (Figure 7B). Similarly, for constructs with H-segments carrying charged or polar flanking residues, we saw a reduction in relative *s*-Mgm1p levels (Figure 7B); the effects of the *pam16-3* mutation were especially large when the charged or polar residues are at the matrix-facing, N-terminal end of the H-segment. It thus appears that a fully functional import motor increases the threshold for H-segment membrane insertion in the context of Mgm1p, possibly by pulling on the nascent chain.

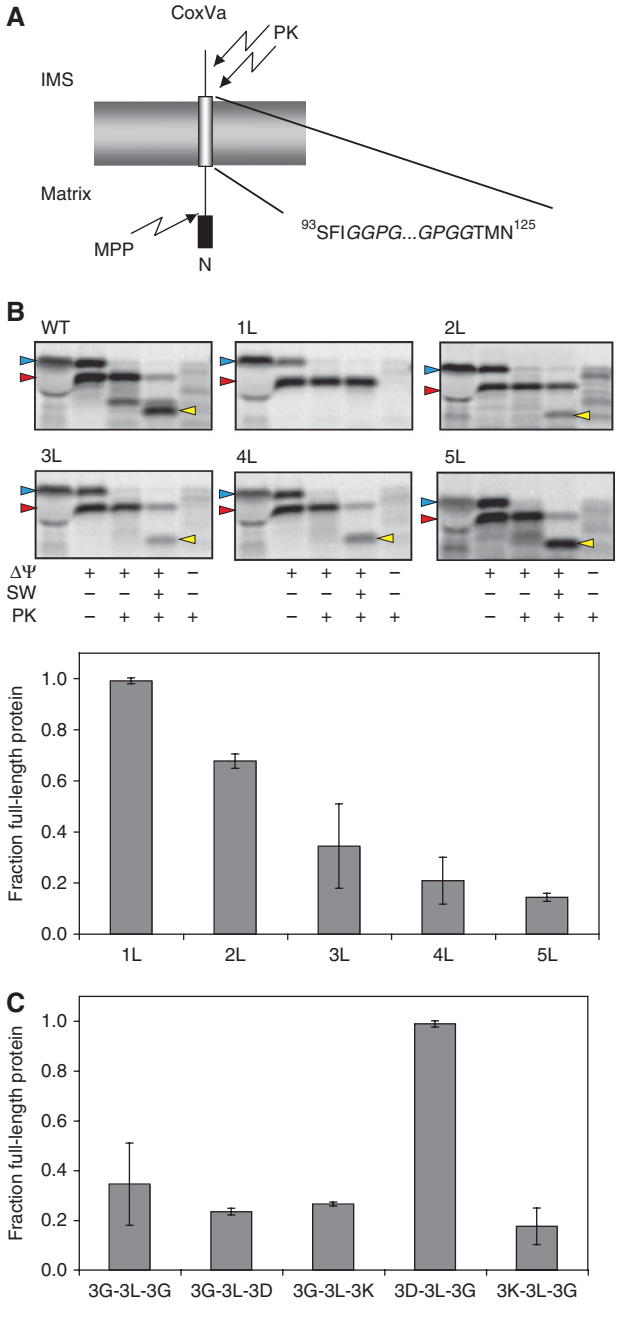

Discussion

In summary, membrane integration of H-segments into the mitochondrial inner membrane depends on overall hydrophobicity and aromatic residues in a similar way as we have found previously for the same set of H-segments in the yeast and mammalian ER membranes (Hessa *et al*, 2007, 2009). Since these characteristics correlate with physicochemical properties of lipid bilayers, the data suggest that protein–lipid interactions contribute in an important way to TM helix integration both in the mitochondrial inner membrane and in the ER membrane.

While the presence of Arg or Lys residues near both the N- and C-terminal ends of the H-segment promotes insertion, the presence of negatively charged or highly polar residues at the matrix-facing, N-terminal end of the H-segment causes a severe defect in membrane integration. This effect is surprisingly strong: in the Mgm1p context, a markedly hydrophobic H-segment such as 11L/8A that is fully integrated into the inner membrane with neutral GGPG…GPGG flanks only

Figure 6 Analysis of H-segments in the context of the CoxVa protein. (**A**) CoxVa has an N-terminal mitochondrial-targeting peptide that is cleaved upon import by the matrix-localized mitochondrial processing peptidase (MPP). A segment consisting of residues 96–122 (containing the single-transmembrane helix in CoxVa) was replaced by GGPG…GPGG-flanked H-segments. If the H-segment is not inserted into the inner membrane but translocated to the matrix, it is protected from proteinase K (PK) treatment, whereas if it is inserted, the C-terminal end will be exposed to the IMS and therefore accessible to PK. (**B**) CoxVa constructs with the indicated H-segments were synthesized in a cell-free translation system in the presence of [^{35}S] methionine and imported into yeast mitochondria. Mitoplasts were prepared by swelling (SW), treated with PK and analysed by SDS–PAGE. A control import reaction was also performed in the presence of valinomycin to dissipate the membrane potential ($\Delta\Psi$). Precursor protein is indicated by a blue arrow, full-length mature protein resulting from MPP cleavage by a red arrow, and PK-trimmed protein by a yellow arrow. Quantitation of the amounts of non-inserted (i.e. translocated), full-length mature protein is shown below the gel images (with standard deviations). (**C**) Amounts of non-inserted, full-length mature protein for 3L/16A H-segments with GGPG…DPDD, GGPG…KPKK, DDPD…GPGG, and KKPK…GPGG flanks. Averages from at least three independent experiments and standard errors are shown.

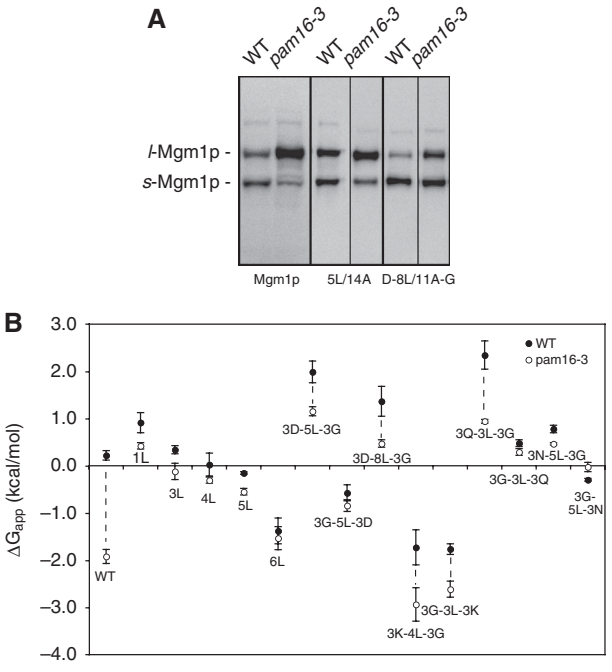

Figure 7 The mitochondrial import motor affects membrane insertion. (**A**) Wild-type Mgm1p and two Mgm1p constructs carrying H-segments GGPG-5L/14A-GPGG and DDPD-8L/11A-GPGG were expressed in the temperature-sensitive *pam16-3* mutant strain and in the isogenic *PAM16* wild-type strain. Yeast transformants were grown at 30°C, and whole-cell lysates were subjected to TCA precipitation followed by SDS–PAGE and western blotting using an anti-HA antibody. The long and short Mgm1p isoforms are indicated. The 5L/14A and D-8L/11A-G lanes are from simultaneous experiments and were assembled from non-neighbouring lanes on the gel. (**B**) ΔG_{app} values for Mgm1p constructs carrying the indicated H-segments. White circles are for the *pam16-3* strain and black circles for the corresponding isogenic wild-type strain. Averages from at least three independent experiments and standard errors are shown.

integrates to about 20% with negatively charged DDPD… flanking residues on the matrix side (Supplementary Table S1, entries #9 and #106; see also the CoxVa constructs #118 and #127). A summary comparison of TM helix recognition and integration in the ER and mitochondrial systems is given in Table I.

What could be the basis for the different effects of positively and negatively charged flanking residues on membrane integration? An obvious possibility is that the electrical potential across the inner membrane, which is negative on the matrix side, could explain the strong reduction in membrane insertion caused by negatively charged residues at the matrix-facing end of a TM segment and the increased insertion efficiency caused by positively charged flanking residues. The reduction in membrane insertion seen when highly polar but uncharged residues replace Gly in the matrix-facing flanking sequences cannot be explained by the membrane potential, however; an interesting possibility is that it may reflect a transbilayer asymmetry in the translocon channel itself.

The positive-inside rule, which states that positively charged residues are more abundant in loops that connect TM segments on the cytoplasmic side (or, in the case of mitochondria, the matrix side), applies to membrane proteins in almost all membranes (Wallin and von Heijne, 1998). However, it has been noted that nuclear-encoded mitochondrial membrane proteins do not always follow the positive-inside rule (Gavel and von Heijne, 1992). Indeed, a statistical analysis of TM segments in mitochondrial membrane proteins that are imported either by the 'conservative sorting' pathway (i.e. they are first translocated into the matrix and then inserted into the inner membrane from the matrix side (Hartl *et al*, 1987)) or by the 'stop-transfer' pathway (i.e. they insert laterally from the TIM23 translocon into the inner membrane (van Loon *et al*, 1986)) shows that, in the latter group, positively charged Lys and Arg residues are abundant on both sides of the TM segments, whereas negatively charged residues seem to be under-represented on the matrix side (Figure 8). This is perfectly consistent with the effects on membrane integration of the Mgm1p and CoxVa constructs uncovered above.

Materials and methods

MGM1 plasmids

The sequence of *MGM1* gene was obtained from Comprehensive Yeast Genome Database (CYGD, Munich information center for protein sequences). This coding region has 21 extra amino acids (MSNSTSLRAIPRVANYNTLVR) at the N-terminus compared with the gene sequence given in UniProt (P32266). The *MGM1* gene was initially amplified by PCR using genomic DNA isolated from yeast strain W303-1a (*MAT a*, *ade2*, *can1*, *his3*, *leu2*, *trp1*, *ura3*) and two primers 5′GTGGTTTGTTACGCATGCAAGCTTGATATCGAAATGAGT AATTCTACTTC3′ and 5′TGGTCTAGAGGTGTAACCACTTGAGTTCTT AGGTAAATTTTTGGAGACGC3′, and subcloned into pJK90 (Kim *et al*, 2003) as described (Kim *et al*, 2006). Then, using two primers 5′CTGGACACCCCTTTTCTG3′ and 5′CAATGGCGTACCCCATAC3′, and pJK90-MGM1 as a template, *MGM1HA* gene was amplified by PCR. This PCR product was subcloned into pHP84HA (Kim *et al*, 2000) by homologous recombination (Oldenburg *et al*, 1997), and this plasmid was named pHP84MGM1HA.

To facilitate subcloning by homologous recombination, a *Sma*I site was generated by an overlap PCR (Spee *et al*, 1993) in the first hydrophobic segment of *MGM1* (^{291}GTGGGTGGCCCCGGGAT GGCT^{309}) in pHP84MGM1HA, and this plasmid was named pJK110. The 19 amino acid long hydrophobic segments (H-segments) were amplified by PCR using various pGEM1-based constructs (Hessa *et al*, 2007) as templates and two primers, 5′ATCTAGTTTGTCCTTAGTAAAAGAGCTAGCTTCTTCTTGTTGCCCT GGTACC3′ and 5′GTTATCACCAGGAGATCGATATCACATTTTCCTA AACTTAAACTTTCCGAGACTAGTG3′ (underlined sequences are the sequences complementing upstream and downstream sequences of *Sma*I restriction enzyme site in pJK110 for homologous recombination, and the rest are the sequences complementing *Escherichia coli* Lep-H-segment sequence). For cloning of constructs #96–97 (KPKK-1L/18A-GPGG and GGPG-1L/18A-KPKK; Supplementary Table S1), available pGEM-based constructs (Lundin *et al*, 2008) were used as PCR templates with the two primers, 5′ATCTAGTTTGTCCTTAGTAAAAGAGCTAGCTTCTTCGCGCCGAAG ACTAGT3′ and 5′GTTATCACCAGGAGATCGATATCACATTTTCCTA AATGACGGGATCGGTAC3′; for these, the five-residue flanks from the Lep vector are APKTS…VPIPS (c.f. Figure 1B). All plasmids carrying an H-segment were constructed by homologous recombination (Oldenburg *et al*, 1997) using a PCR amplified *E. coli* Lep-H-segment and a *Sma*I-digested pJK110 with Δ*mgm1a* or α strains (*MATa or α his3Δ 1; leu2Δ0*; *ura3Δ0*; *mgm1*::*kanMX4*) (Westermann and Neupert, 2000). Plasmids were isolated from yeast transformants, the correct sequences were confirmed by DNA sequencing. Correct constructs were then re-transformed into W303-1a (*MAT a*, *ade2*, *can1*, *his3*, *leu2*, *trp1*, *ura3*), selected on –Leu plates, and these yeast transformants were subjected to further analysis.

For *in vitro* expression of the full-length *p*-Mgm1p and *p*-Mgm1p-6L/13A with a presequence (residues 1–902 plus triple-HA tag), the DNA fragments were amplified by PCR using a pHP84MGM1HA or pHP84MGM1(6L/13A)HA as a template and the 3′ end primer 5′TTAGAGAGCGTAATCTGGAAC3′ and 5′ end primer 5′ATGA

Table I Comparison of H-segment recognition by the Sec61 versus the TIM23 translocons

	Sec61 translocon in the ER	TIM23 complex in the mitochondrial inner membrane
Threshold hydrophobicity of the H-segment	$n=3$ (Dog pancreas RM), $n=5$ (yeast ER) in GGPG-*n*L/(19-*n*)A-GPGG H-segment	$n=3$ (CoxVa), $n=6$ (Mgm1p) in GGPG-*n*L/(19-*n*)A-GPGG H-segment
Effect of Pro residues in the H-segment	Ala→Pro replacements in the N-terminal three positions and the most C-terminal position decrease membrane insertion less than Ala→Pro replacements in the middle of the H-segment	Qualitatively similar to the ER
Effect of aromatic residues in the H-segment	Ala→Trp, Tyr replacements increase membrane insertion when near the N- or the C-terminus of the H-segment, but decrease insertion when in the middle of the H-segment	Same as in the ER
Effect of positively charged residues in the H-segment	Ala→Lys, Arg most unfavourable for membrane insertion when placed in the middle part of the H-segment	Same as in the ER
Effect of negatively charged residues in the H-segment	Ala→Asp, Glu most unfavourable for membrane insertion when placed in the middle part of the H-segment	Ala→Asp, Glu most unfavourable for membrane insertion when placed in the middle and N-terminal (matrix-facing) part of the H-segment
Effect of negatively charged flanking residues	DDPD… and EEPE… flanks decrease membrane insertion compared with GGPG… flank when placed next to the lumenal end of the H-segment	DDPD… and EEPE… flanks decrease membrane insertion compared with GGPG… flank when placed next to the matrix end of the H-segment
Effect of positively charged flanking residues	…KPKK and …RPRR flanks increase membrane insertion compared with …GPGG flank when placed next to the cytoplasmic end of the H-segment	KKPK…KPKK and RRPR…RPRR flanks increase membrane insertion compared with GGPG…GPGG flanks when placed next to both the IMS and matrix ends of the H-segment

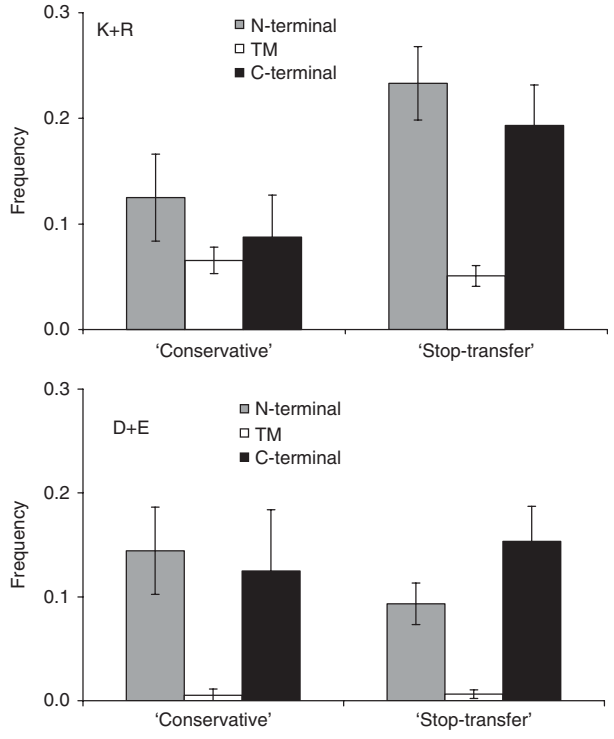

Figure 8 Mean frequencies of positively (K + R, top panel) and negatively (D + E, bottom panel) charged residues in the 10 residues flanking the transmembrane segments on the matrix side (grey bars), in the transmembrane segment (white bars), and in the 10 residues flanking the transmembrane segment on the intermembrane space (IMS) side (black bars) in a collection of transmembrane segments in mitochondrial proteins imported via a 'conservative' sorting mechanism in which the protein is first fully imported into the matrix and then inserted into the inner membrane from the matrix side (eight proteins, see Materials and methods), or via a 'stop-transfer' mechanism in which the transmembrane segment is arrested in the TIM23 translocon and inserted laterally into the inner membrane (21 proteins). Standard errors are shown.

GTAATTCTACTTC3′. The PCR products were subcloned into a TOPO blunt end vector (Invitrogen) according to the manufacturer's protocol. Correct insertion into the vector was confirmed by restriction enzyme digestion analysis.

In vitro translation

p-Mgm1HAp and *p*-Mgm1p-6L/13AHAp were expressed *in vitro* following the manufacturer's protocol for the T7 reticulolysate coupled transcription and translation system (Promega). Whole-cell lysate samples from yeast transformants expressing HA-tagged Mgm1p and Mgm1p(6L/13A) (see below) were subjected to TCA precipitation and analysed by SDS–PAGE and western blotting against an anti-HA antibody.

Western blot analysis

Yeast transformants carrying various *MGM1HA* H-segments were grown overnight in 5 ml of –Leu medium at 30°C and harvested by centrifugation at 3000 *g*. Whole-cell lysate preparation, SDS–PAGE, and western blotting using an antibody against the HA tag were done as described (Kim *et al*, 2006). Western blots were developed on a Fuji LAS-3000 system and the bands were quantitated using the Image Gauge V 3.45 software.

The temperature-sensitive mutant strain *pam16-3* and the *PAM16* isogenic wild-type strain (Frazier *et al*, 2004) were kind gifts from Dr Nikolaus Pfanner, Freiburg. *MGM1HA* carrying various H-segments were transformed into the *pam16-3* and the isogenic wild-type strains. Yeast transformants were grown at 30°C as described above. Whole-cell lysates were subjected to TCA precipitation before loading on to the SDS gels. Western blotting and quantitation were done as described above.

CoxVa plasmids

The *COXVa*-coding sequence was amplified by PCR using the primers coxVa(*Eco*RI)F (5′CCGAATTCTGCACCAAACACAAGATCA ACTAAGAACGC3′ and coxVa(*Bam*HI)R (5′CCGGATCCCCTATTGATT TCCTTTCAAAATTTCTGGCC3′). The PCR fragment was treated with *Eco*RI and *Bam*HI and inserted between *Eco*RI/*Bam*HI-digested pGEM4z vector (Promega). *COXVa* H-segment constructs were made by overlap PCR using the primer pair SP6 5′ATTTAGGTGA CACTATAG3′ and: CoxVa(P2)R 5′TAAGCGCAGACCAGTCGGCCA TTCGCCTTCTTGCTTATCTCCAGGACCACCAATAAAACTGGAATC3′; CoxVa(Mgm1p)R 5′AGCCATCCCGCCACCCACATATATGGGTAACC TAATAATTTTAGATATAATAATAAAACTGGAATC3′; CoxVa(8L/11A)R 5′CAGTAGGAGAAGCAATAACAGTGCGGCGGCAGCAGCTGCTCCAGG ACCACCAATAAAACTGGAATC3′; CoxVa(5L/14A)R 5′AAGAGCTGC AAGTGCTGCTAAAGCTAATGCTGCAGCTGCTCCAGGACCACCAATA AAACTGGAATC3′ and the primer pair T7 5′TAATACGACTCACTATA GGG3′ and: CoxVa(P2) 5′TGGCCGACTGGTCTGCGCTTAAGTCGA ATTGGCGGCATCGGACCTGGTGGGACCATGAATAAGGAG3′; CoxVa (Mgm1p) 5′TATGTGGGTGGCGGGATGGCTGCTGCAGGGAGTTATAT AGCTTATAAGATGACCATGAATAAGGAG3′; CoxVa(8L/11A) 5′CTGT TATTGCTTCTCCTACTGTTAGCTGCCGCTGCTGCAGGACCTGGTGGG ACCATGAATAAGGAG3′; CoxVa(5L/14A) 5′TTAGCAGCACTTGCAGC TCTTGCACTAGCTGCAGCAGCTGGACCTGGTGGGACCATGAATAAGG AG3′. The resulting fragments were cloned into the pGEM4z vector (Promega) by *Eco*RI/*Bam*HI digestion. The constructs CoxVa(1L/18A), CoxVa(2L/17A), CoxVa(3L/16A), and CoxVa(4L/15A) were obtained by site-directed mutagenesis using construct CoxVa(5L/14A) as template. The constructs CoxVa(KKPK-3L/16A-GPGG), CoxVa(GGPG-3L/16A-KPKK), CoxVa(DDPD-3L/16A-GPGG), and CoxVa(GGPG-3L/16A-DPDD) were obtained by site-directed mutagenesis using construct CoxVa(3L/16A) as template. Constructs CoxVa(DDPD-5L/14A-GPGG), CoxVa(DDPD-8L/11A-GPGG), and CoxVa(KKPK-1L/18A-GPGG) were obtained by site-directed mutagenesis using constructs CoxVa(5L/14A), CoxVa(8L/11A) and CoxVa(1L/18A) as template.

Analysis of CoxVa H-segment constructs

The radiolabelled precursor proteins were synthesized in a cell-free translation system with rabbit reticulocyte lysate (Promega) in the presence of [^{35}S] methionine. Isolated mitochondria from the yeast wild-type strain W3031-1a were incubated with radiolabelled precursor proteins in import buffer (250 mM sucrose, 10 mM MOPS-KOH, pH 7.2, 80 mM KCl, 5 mM $MgCl_2$, 2.5 mm potassium phosphate, 2 mM ATP, 2 mM methionine, 2 mM NADH, and 1% (w/v) bovine serum albumin) at 25°C. The import reaction was stopped by addition of 10 μg/ml valinomycin. Mitoplasts were prepared by diluting mitochondria 10-fold in EM buffer (10 mM MOPS-KOH, pH 7.2, 1 mM EDTA). Protease treatment was performed by incubating the mitochondria (or mitoplasts) with 100 μg/ml proteinase K for 20 min on ice, which was inactivated by subsequent addition of 1 mM PMSF. Mitochondria (or mitoplasts) were reisolated by centrifugation, and proteins were analysed by SDS–PAGE and radioimaging with a Typhoon Variable Mode Imager 9200 (GE Healthcare) or Pharos FX Plus Molecular Imager (Bio-Rad).

Calculation of ΔG_{app}

Membrane integration of each H-segment was quantified from western blots by measuring relative amounts of *l*-Mgm1p and *s*-Mgm1p isoforms. The relative amounts of the two isoforms were used to calculate an apparent equilibrium constant between the membrane integrated and non-integrated forms: $K_{app} = f_l/f_s$, where f_l is the fraction of membrane integrated and f_s is the fraction of membrane non-integrated isoforms. Finally, the membrane insertion efficiency was expressed as an apparent free energy difference, $\Delta G_{app} = -RT\ \ln K_{app}$. The 'biological' ΔG^X_{app} scale for the 20 individual amino acids (X) was derived from a simple additive model, $\Delta G^X_{app} = \Delta G_{app} - (n \cdot \Delta G^{Leu}_{app} + (18 - n) \cdot \Delta G^{Ala}_{app})$, where ΔG_{app} is the measured insertion free energy of the construct in question (see Supplementary Table S1). At least three independent experiments were carried out for each H-segment to measure ΔG_{app}.

Statistical analysis of TM segments in mitochondrial inner membrane proteins

Two sets of (mostly single spanning) TIM23-dependent mitochondrial inner membrane proteins were analysed, one containing eight proteins known to be first imported into the matrix and then inserted by the 'conservative sorting' pathway into the inner membrane from the matrix side, and the other containing 21 proteins that are inserted laterally by the 'stop-transfer' pathway from the TIM23 translocon into the inner membrane; see Supplementary Table S2 for sequence identifiers and references.

To analyse the charge distribution in the regions flanking the TM segments, the 10 N- and C-terminal residues flanking each TM segment (as predicted by SCAMPI (Bernsel *et al*, 2008)) were extracted. The mean frequencies of positively charged (R + K) and negatively charged residues (D + E) were calculated for the N- and C-terminal segments, along with the standard error of the mean.

Supplementary data

Supplementary data are available at *The EMBO Journal* Online (http://www.embojournal.org).

Acknowledgements

This work was supported by grants from the Swedish Cancer Foundation, the Swedish Research Council, the Swedish Foundation for Strategic Research, and the European Research Council (ERC-2008-AdG 232648) to GvH, from the Research Settlement Fund for the new faculty of SNU and the National Research Foundation of Korea (NRF 0409-20100093) to HK, and from the Deutsche Forschungsgemeinschaft SFB 594 project B8 and the Cluster of Excellence 'Macromolecular Complexes' at the Goethe University Frankfurt DFG Project EXC 115 to ASR. KY and TE acknowledge support of this work by Grants-in-Aid for Scientific Research from the Ministry of Education, Culture, Sports, Science and Technology of Japan (MEXT). SCB is a recipient of a graduate student fellowship (SFRH/BD/36107/2007) from Fundação para a Ciência e a Tecnologia, Portugal.

Conflict of interest

The authors declare that they have no conflict of interest.

References

Becker T, Gebert M, Pfanner N, van der Laan M (2009) Biogenesis of mitochondrial membrane proteins. *Curr Opin Cell Biol* **21:** 484–493

Bernsel A, Viklund H, Falk J, Lindahl E, von Heijne G, Elofsson A (2008) Prediction of membrane-protein topology from first principles. *Proc Natl Acad Sci USA* **105:** 7177–7181

Bolender N, Sickmann A, Wagner R, Meisinger C, Pfanner N (2008) Multiple pathways for sorting mitochondrial precursor proteins. *EMBO Rep* **9:** 42–49

Dolezal P, Likic V, Tachezy J, Lithgow T (2006) Evolution of the molecular machines for protein import into mitochondria. *Science* **313:** 314–318

Frazier AE, Dudek J, Guiard B, Voos W, Li Y, Lind M, Meisinger C, Geissler A, Sickmann A, Meyer HE, Bilanchone V, Cumsky MG, Truscott KN, Pfanner N, Rehling P (2004) Pam16 has an essential role in the mitochondrial protein import motor. *Nat Struct Mol Biol* **11:** 226–233

Gavel Y, von Heijne G (1992) The distribution of charged amino acids in mitochondrial inner membrane proteins suggests different modes of membrane integration for nuclearly and mitochondrially encoded proteins. *Eur J Biochem* **205:** 1207–1215

Glaser SM, Miller BR, Cumsky MG (1990) Removal of a hydrophobic domain within the mature portion of a mitochondrial inner membrane protein causes its mislocalization to the matrix. *Mol Cell Biol* **10:** 1873–1881

Hartl FU, Ostermann J, Guiard B, Neupert W (1987) Successive translocation into and out of the mitochondrial matrix: targeting of proteins to the intermembrane space by a bipartite signal peptide. *Cell* **51:** 1027–1037

Herlan M, Bornhovd C, Hell K, Neupert W, Reichert AS (2004) Alternative topogenesis of Mgm1 and mitochondrial morphology depend on ATP and a functional import motor. *J Cell Biol* **165:** 167–173

Herlan M, Vogel F, Bornhovd C, Neupert W, Reichert AS (2003) Processing of Mgm1 by the rhomboid-type protease Pcp1 is required for maintenance of mitochondrial morphology and of mitochondrial DNA. *J Biol Chem* **278:** 27781–27788

Herrmann JM (2003) Converting bacteria to organelles: evolution of mitochondrial protein sorting. *Trends Microbiol* **11:** 74–79

Hessa T, Kim H, Bihlmaier K, Lundin C, Boekel J, Andersson H, Nilsson I, White SH, von Heijne G (2005) Recognition of transmembrane helices by the endoplasmic reticulum translocon. *Nature* **433:** 377–381

Hessa T, Meindl-Beinker NM, Bernsel A, Kim H, Sato Y, Lerch-Bader M, Nilsson I, White SH, von Heijne G (2007) Molecular code for transmembrane-helix recognition by the Sec61 translocon. *Nature* **450:** 1026–1030

Hessa T, Reithinger JH, von Heijne G, Kim H (2009) Analysis of transmembrane helix integration in the endoplasmic reticulum in S. cerevisiae. *J Mol Biol* **386:** 1222–1228

Kim H, Österberg M, Melén K, von Heijne G (2006) A global topology map of the *Saccharomyces cerevisiae* membrane proteome. *Proc Natl Acad Sci USA* **103:** 11142–11147

Kim H, Park H, Montalvo L, Lennarz WJ (2000) Studies on the role of the hydrophobic domain of Ost4p in interactions with other subunits of yeast oligosaccharyl transferase. *Proc Natl Acad Sci USA* **97:** 1516–1520

Kim H, Yan Q, von Heijne G, Caputo GA, Lennarz WJ (2003) Determination of the membrane topology of Ost4p and its subunit interactions in the oligosaccharyltransferase complex in *Saccharomyces cerevisiae*. *Proc Natl Acad Sci USA* **100:** 7460–7464

Llopis J, McCaffery JM, Miyawaki A, Farquhar MG, Tsien RY (1998) Measurement of cytosolic, mitochondrial, and Golgi pH in single living cells with green fluorescent proteins. *Proc Natl Acad Sci USA* **95:** 6803–6808

Lundin C, Kim H, Nilsson I, White SH, von Heijne G (2008) Molecular code for protein insertion in the endoplasmic reticulum membrane is similar for N(in)-C(out) and N(out)-C(in) transmembrane helices. *Proc Natl Acad Sci USA* **105:** 15702–15707

Meeusen S, DeVay R, Block J, Cassidy-Stone A, Wayson S, McCaffery JM, Nunnari J (2006) Mitochondrial inner-membrane fusion and crista maintenance requires the dynamin-related GTPase Mgm1. *Cell* **127:** 383–395

Meier S, Neupert W, Herrmann JM (2005) Proline residues of transmembrane domains determine the sorting of inner membrane proteins in mitochondria. *J Cell Biol* **170:** 881–888

Miller BR, Cumsky MG (1993) Intramitochondrial sorting of the precursor to yeast cytochrome c oxidase subunit Va. *J Cell Biol* **121:** 1021–1029

Neupert W, Herrmann JM (2007) Translocation of proteins into mitochondria. *Annu Rev Biochem* **76:** 723–749

Oldenburg KR, Vo KT, Michaelis S, Paddon C (1997) Recombination-mediated PCR-directed plasmid construction *in vivo* in yeast. *Nucleic Acids Res* **25:** 451–452

Rapoport TA (2007) Protein translocation across the eukaryotic endoplasmic reticulum and bacterial plasma membranes. *Nature* **450:** 663–669

Schäfer A, Zick M, Kief J, Steger M, Heide H, Duvezin-Caubet S, Neupert W, Reichert AS (2010) Intramembrane proteolysis of Mgm1 by the mitochondrial rhomboid protease is highly promiscuous regarding the sequence of the cleaved hydrophobic segment. *J Mol Biol* **401:** 182–193

Sesaki H, Jensen RE (2004) Ugo1p links the Fzo1p and Mgm1p GTPases for mitochondrial fusion. *J Biol Chem* **279:** 28298–28303

Sesaki H, Southard SM, Yaffe MP, Jensen RE (2003) Mgm1p, a dynamin-related GTPase, is essential for fusion of the mitochondrial outer membrane. *Mol Biol Cell* **14:** 2342–2356

Skach WR (2009) Cellular mechanisms of membrane protein folding. *Nat Struct Mol Biol* **16:** 606–612

Spee JH, de Vos WM, Kuipers OP (1993) Efficient random mutagenesis method with adjustable mutation frequency by use of PCR and dITP. *Nucleic Acids Res* **21:** 777–778

van Loon A, Brändli A, Schatz G (1986) The presequences of two imported mitochondrial proteins contain information for intracellular and intramitochondrial sorting. *Cell* **44:** 801–812

Wallin E, von Heijne G (1998) Genome-wide analysis of integral membrane proteins from eubacterial, archaean, and eukaryotic organisms. *Protein Sci* **7:** 1029–1038

Westermann B, Neupert W (2000) Mitochondria-targeted green fluorescent proteins: convenient tools for the study of organelle biogenesis in Saccharomyces cerevisiae. *Yeast* **16:** 1421–1427

Wong ED, Wagner JA, Scott SV, Okreglak V, Holewinske TJ, Cassidy-Stone A, Nunnari J (2003) The intramitochondrial dynamin-related GTPase, Mgm1p, is a component of a protein complex that mediates mitochondrial fusion. *J Cell Biol* **160:** 303–311

Zick M, Duvezin-Caubet S, Schafer A, Vogel F, Neupert W, Reichert AS (2009) Distinct roles of the two isoforms of the dynamin-like GTPase Mgm1 in mitochondrial fusion. *FEBS Lett* **583:** 2237–2243